Available at www.sciencedirect.com

ScienceDirect

journal homepage: www.elsevier.com/locate/watres

Electrochemical degradation of the β-blocker metoprolol by $Ti/Ru_{0.7}Ir_{0.3}O_2$ and Ti/SnO_2-Sb electrodes

Jelena Radjenovic [a,*], *Beate I. Escher* [b], *Korneel Rabaey* [a]

[a] *The University of Queensland, Brisbane, QLD Advanced Water Management Centre, 4072, Australia*
[b] *The University of Queensland, Brisbane, National Research Centre for Environmental Toxicology (Entox), QLD 4108, Australia*

ARTICLE INFO

Article history:
Received 7 February 2011
Received in revised form
21 March 2011
Accepted 21 March 2011
Available online 29 March 2011

Keywords:
Electrochemical oxidation
Bioassays
Halogenated by-product
Micropollutant

ABSTRACT

Electrochemical oxidation has been proposed for the elimination of pesticides, pharmaceuticals and other organic micropollutants from complex waste streams. However, the detrimental effect of halide ion mediators and the generation of halogenated by-products in this process have largely been neglected thus far. In this study, we investigated the electrochemical oxidation pathways of the β-blocker metoprolol in reverse osmosis concentrate (ROC) from a water reclamation plant using titanium anodes coated with $Ru_{0.7}Ir_{0.3}O_2$ or SnO_2-Sb metal oxide layers. The results of liquid chromatography-mass spectrometry analysis indicated that irrespective of the electrode coating the same oxidant species participated in electrochemical transformation of metoprolol in ROC. Although Ti/SnO_2-Sb exhibited higher oxidizing power for the same applied specific electrical charge, the generation of large fractions of chloro-, chloro-bromo- and bromo derivatives was observed for both electrode coatings. However, degradation rates of metoprolol and its degradation products were generally higher for the Ti/SnO_2-Sb anode. Chemical analyses of metoprolol and its by-products were complemented with bioanalytical tools in order to investigate their toxicity relative to the parent compound. Results of the bioluminescence inhibition test with *Vibrio fischeri* and the combined algae test with *Pseudokirchneriella subcapitata* indicated a substantial increase in non-specific toxicity of the reaction mixture due to the formed halogenated by-products, while the specific toxicity (inhibition of photosynthesis) remained unchanged.

1. Introduction

The unique ability of electrochemical processes to oxidize and/or reduce organic compounds at controlled electrode potentials and using only electrons as reagents represents a great advantage over existing advanced oxidation processes (AOPs). Due to the generation of a variety of reactive oxygen species (ROS) at the anode (e.g. OH•, H_2O_2, O_2, O_3), electrochemical oxidation is considered to be versatile and capable of oxidizing persistent organic micropollutants, nitrogen species and microorganisms (Comninellis et al., 2010). In recent years, there has been an increasing interest in applying electrochemical oxidation for the treatment of refractory waste streams such as landfill leachate and reverse osmosis concentrate (ROC) from water treatment processes (Anglada et al., 2009; Van Hege et al., 2004; Dialynas et al., 2008; Perez et al., 2010). Due to the high concentrations of organic contaminants, disposal of these streams represents a major problem as they require an on-site treatment. High concentrations of Cl^- ions in landfill leachate and ROC not only promote indirect oxidation via reactive

* *Corresponding author*. Tel.: +61 7 3346 3234; fax: +61 7 3365 4726.
E-mail address: j.radjenovic@awmc.uq.edu.au (J. Radjenovic).
0043-1354/$ – see front matter © 2011 Elsevier Ltd. All rights reserved.
doi:10.1016/j.watres.2011.03.040

halogen species (RHS) (e.g. Cl_2/ClO^-, ClO_2), they also lower the ohmic resistance of the system making it more energy-efficient. However, the main issue raised among environmental electrochemists is their detrimental effect on the outcome of oxidation due to the generation of chlorinated by-products.

The scenario with a plurality of different ROS generated during electrochemical oxidation is already very complex, and besides ROS it will involve a number of different radical and non-radical RHS in the Cl^- containing solutions. Generally, it is considered that the formation and distribution of electrochemical oxidation by-products is also governed by the oxidizing power of an anode and applied potential. The oxidizing power is determined by the anode overpotential toward the oxygen evolution reaction and adsorption enthalpy of the electrogenerated OH• (Comninellis et al., 2010). Anodes such as boron-doped diamond, Ti/SnO_2-Sb, Ti/PbO_2 are characterized by a high overpotential for the oxygen evolution reaction. They are capable of combusting organic compounds and are usually referred to as non-active anodes (i.e. with weak electrode-OH• interaction). Anodes such as Ti/IrO_2 and Ti/RuO_2 have a lower oxidizing power and rather promote selective oxidation, i.e. conversion rather than degradation. These electrodes have a strong interaction with the generated OH• and are called active anodes. Extensive investigation has been performed on the electrochemical oxidation of specific organic micropollutants in supporting electrolytes (e.g. Na_2SO_4, KH_2PO_4, NaCl) using active and non-active electrodes. Recent studies have addressed the formation of low molecular weight halogenated by-products such as trihalomethanes and haloacetic acids during electrochemical oxidation of landfill leachate (Anglada et al., 2011) and ROC (Perez et al., 2010; Bagastyo et al., 2011). However, to the author's knowledge, no investigation has been done on the oxidative transformations of organic micropollutants in real waste streams, and hence the effects of a complex matrix with high chloride content on the formation of degradation products have not been established. In this study, the electrochemical oxidation pathways of a model organic micropollutant, the β-blocker metoprolol, were investigated in a real ROC matrix. Metoprolol is used for the treatment of a range of cardiac conditions such as hypertension, angina and arrhythmias, and it is commonly found in wastewater effluents and surface water (Hernando et al., 2007). The experiments were performed using two electrodes coated with active and non-active layers of $Ru_{0.7}Ir_{0.3}O_2$ and SnO_2-Sb, respectively, at two current densities. The ability of a hybrid triple quadrupole-linear ion trap mass spectrometer to establish fragmentation pathways in MS^3 sequential product ion spectra experiments enabled elucidation of electrochemical oxidation pathways and identification of metoprolol by-products. Given that not all by-products can be readily quantified by chemical analysis, we additionally evaluated the toxicity of the reaction mixture (ROC alone and ROC spiked with metoprolol) during electrochemical oxidation in bioluminescence inhibition tests (Microtox) using the marine bacterium *Vibrio fischeri*, and a combined algae test with *Pseudokirchneriella subcapitata*, respectively. The combined algae test was chosen as previous work indicated a high algal toxicity of β-blockers (Neuwoehner and Escher, 2011; Escher et al., 2006).

2. Materials and methods

2.1. Chemicals, media and setup

Metoprolol tartarate (analytical grade, ≥99%) was purchased from Sigma-Aldrich (U.S.A.). All solvents (methanol, acetonitrile and water) as well as formic acid (98%) were HPLC-grade (Merck, Germany). The ROC used in the experiments was sampled at an advanced water treatment plant (AWTP) in Bundamba, 30 km west of Brisbane, Australia. This AWTP receives a mixture of secondary treated effluents from four wastewater treatment plants. After pretreatment of the secondary effluents (addition of iron coagulants, separation of solids in the clarifier), water is passed through microfiltration and reverse osmosis membranes before being treated with hydrogen peroxide/UV advanced oxidation and chemical stabilization and desinfection. The ROC was obtained straight after the reverse osmosis step. The concentrations of chloride and bromide ions in ROC were measured to be 1.65 g L^{-1} and 1.48 mg L^{-1}, respectively.

The electrochemical cell was constructed by assembling two equal rectangular polycarbonate frames with internal dimensions of 20 × 5 × 1.2 cm. The frames were bolted together between two rectangular polycarbonate plates. The anode cell was separated from the cathode cell by a cation exchange membrane (Ultrex CMI-7000, Membranes International, U.S.A.). Sealing was ensured by a rubber o-ring inserted between the two frames. The net volume for each compartment was 114 mL. As anodes, either a Ti/$Ru_{0.7}Ir_{0.3}O_2$ electrode or a Ti/SnO_2-Sb electrode was used, both with 12 g m^{-2} coating on the Ti mesh (dimensions: 4.8 × 5 cm; thickness: 1 mm; specific surface area: 1.0 m^2 m^{-2}), supplied by Magneto Special Anodes (The Netherlands). The cathode used was a woven stainless steel mesh (dimensions: 4.8 × 5 cm; 80 μm × 0.050 mm wire diameter), both the anode and cathode had a projected electrode surface area of 24 cm^2. For electrochemical control, a Wenking potentiostat/galvanostat (KP07, Bank Elektronik, GmbH, Pohlheim, Germany) was used. The anodic half-cell potentials were measured by placing an Ag/AgCl reference electrode (assumed +0.197 V vs SHE) in the anode compartment. Data was recorded every 60 s using an Agilent 34970A data acquisition unit (Agilent Technologies, U.S.A.). For the anode, a recirculation was foreseen at 162 mL min^{-1}, on a 1 or 10 L buffer vessel. Likewise, cathode medium (0.1 M HCl) was recirculated at 162 mL min^{-1} over a 1 or 10 L buffer vessel.

2.2. Experimental approach

To investigate the electrochemical oxidation pathways of metoprolol (MTPL), 1 L of ROC collected prior to the nitrification stage was amended with the target compound dissolved in water to a final concentration of MTPL of 50 μM. The spiked ROC was then recirculated over the electrochemical cell over a period of 3 h, at current densities $J = 100$ and 250 A m^{-2} using Ti/$Ru_{0.7}Ir_{0.3}O_2$ or a Ti/SnO_2-Sb electrode. The system was operated in batch mode, with 1 mL samples taken every 5–15 min during the 3 h experiment.

To determine the toxicity of formed by-products relative to the parent compound, 10 L of the same ROC matrix containing

MTPL (50 μM) was oxidized in batch mode using the same reactor and the Ti/SnO_2-Sb anode, at $J = 250$ A m^{-2}. 100 mL samples were taken after 2, 4, 6, 8, 10 and 24 h and extracted by a previously optimized solid phase extraction (SPE) method (Radjenovic et al., 2010). Analysis of sample extracts used in bioassays enabled assignment of the observed ecotoxic effect to a mixture of specific, newly identified by-products. All experiments were performed in duplicate under galvanostatic control, at room temperature (25 ± 1 °C).

2.3. *Sample preparation*

As a variety of generated oxidants can prevent efficient sample stabilization, no quenching agent was added to the sample, and samples were immediately stored at −20 °C. Quenching of free chlorine may lead to errors in analytical determination of trace organics due to the formation of the original compounds from their N-chloro analogs (Wulfeck-Kleier et al., 2010). In the experiment performed to determine the toxicity of MTPL by-products, solid phase extraction (SPE) of electrochemically oxidized samples was performed. The sample pH was adjusted immediately after sampling to pH 7 by adding an appropriate amount of 0.1 M NaOH, and 100 mL samples were extracted on a Visiprep manifold system (Sigma-Aldrich, U.S.A.) using Oasis HLB cartridges (200 mg, 6 ml) from Waters Corporation (U.S.A.), previously conditioned with 10 mL of methanol and 10 mL of deionized water (HPLC-grade). Chloride and bromide ions were measured by ion chromatography (IC)-Dionex 2010i (Dionex, U.S.A.).

2.4. *Chemical analysis*

Liquid chromatography-mass spectrometry (LC-MS) analyses were performed using a Shimadzu Prominence ultra-fast liquid chromatography (UFLC) system (Shimadzu, Japan) coupled with a 4000 QTRAP quadrupole-linear ion trap mass spectrometer (QqLIT-MS) equipped with a Turbo Ion Spray source (Applied Biosystems-Sciex, U.S.A.). Chromatographic separation was achieved with an Alltima C18 Column (250 × 4.6 mm, particle size 5 μm) run at 40 °C, supplied by Alltech Associates Inc (U.S.A.).

The structure of electrochemical oxidation by-products of MTPL was elucidated by isolating the protonated molecular ions, collision induced dissociation (CID) MS^2 and MS^3 experiments in (+)ESI mode and mass spectral comparison with the parent compound. Additional confirmation of the identity was obtained by the retention time (t_R) and isotope abundance and distribution that enabled confirmation of halogenated intermediates. Detailed description of the recorded mass spectra is given in the Supporting Information.

2.5. *Microtox and* Pseudokirchneriella subcapitata *bioassays*

The Microtox assay with *Vibrio fischeri* and the combined algae test with the green algae *Pseudokirchneriella subcapita* were performed as described previously (Escher et al., 2008), on the samples pre-treated by SPE. Three endpoints were assessed in the combined algae test: the direct inhibition of photosynthesis after 2 h and 24 h incubation via measurement of the quantum yield of photosystem II using Imaging pulse-amplitude modulated fluorometry (2 h IPAM and 24 h IPAM) and the inhibition of growth rate (24 h growth rate). The effect concentrations causing 50% of maximum effect (EC_{50}) were derived for all endpoints from full concentration-response curves and were expressed in units of relative enrichment factor (REF). The results of the Microtox and the endpoint of 24 h algal growth rate inhibition were additionally converted to baseline-toxicity equivalent concentration (baseline-TEQ) relative to a virtual reference compound with an EC_{50} of 12.2 mg L^{-1} in the Microtox and 18.75 mg/L in the algae test (Escher et al., 2008).

3. Results and discussion

In the first part of this work, four different experiments were conducted using 1 L of ROC amended with MTPL and Ti/$RuIrO_2$ and Ti/SnO_2-Sb electrode operating at $J = 100$ and 250 A m^{-2}. Samples from these experiments were all scanned in full-scan mode and identification of unknown by-products was performed as described in Chemical analysis section. The measured anode potentials (E_{AN}) of Ti/$RuIrO_2$ and Ti/SnO_2-Sb were 1.77 ± 0.1 and 2.25 ± 0.06 V vs Ag/AgCl, respectively. No electrode passivation was observed in any of the experiments conducted. The anolyte pH decreased from the initial pH 7.75 ± 0.1 to pH 3.4 ± 0.15 ($J = 100$ A m^{-2}) and 2.4 ± 0.1 ($J = 250$ A m^{-2}) using Ti/$RuIrO_2$ anode, and to pH 2.7 ± 0.2 ($J = 100$ A m^{-2}) and 2.2 ± 0.1 ($J = 250$ A m^{-2}) using Ti/SnO_2–Sb anode.

3.1. *Structural elucidation of electrochemical oxidation products of MTPL*

In the full-scan experiments recorded in the range *m/z* 100–600 several new peaks appeared during the course of the oxidation experiment with retention time (t_R) lower than the one observed for MTPL ($t_R = 10.1$ min). Four new peaks eluting at $t_R = 2.8$, 7.2, 7.9 and 8.7 min were assigned to molecular ions *m/z* 134 (P133), 254 (P253), 238 (P237) and 226 (P225), respectively (Table S1, Fig. 2). Products P225 (formed by N-dealkylation of MTPL) and P253 (formed by the cleavage of terminal methyl group) were previously reported as ozonation products of MTPL (Benner and Ternes, 2009), while P237 (formed by the cleavage of the terminal methoxy group) was one of the main products of e-beam and γ-radiolysis of MTPL (Slegers et al., 2006). On the other hand, in CID experiments molecular ion *m/z* 134 was identified as a polar intermediate P133, formed by the cleavage of aromatic ether bond in the MTPL molecule (Figure S1). Next, the same nominal mass of two molecular ions at *m/z* 284 (mass shift of +16 Da) and their elution at $t_R = 6.1$ and 6.8 min suggested the attachment of −OH group in different positions in the MTPL molecule, leading to different polarities of the formed intermediates. The mass spectra of these two products marked as P283-I and P283-II, respectively, are identical to the ones reported in Benner and Ternes (2009) and Slegers et al. (2006). Thus implies that the hydroxylation occurred at the benzene ring and at the β-carbon in the methoxyethyl side chain, respectively. Besides the P283-II, product P281-II ($t_R = 6.95$ min, *m/z*

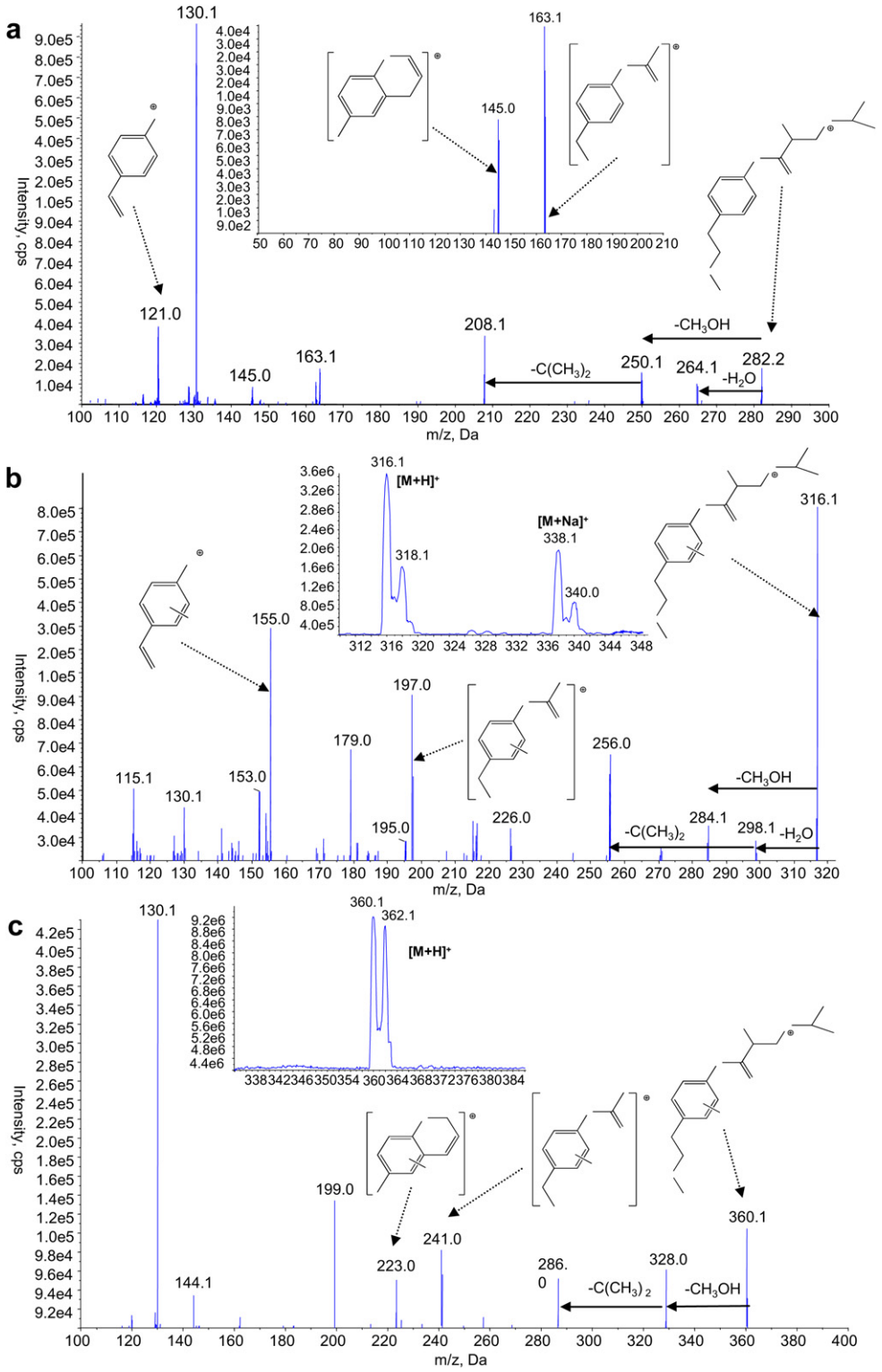

Fig. 1 – a) (+)ESI-QqLIT-MS^2 spectrum of P281, protonated molecular ion, $[M + H]^+$, at *m/z* 282; insert: (+)ESI-QqLIT-MS^3 spectrum: *m/z* 282→*m/z* 208, b) (+)ESI-QqLIT-MS^2 spectrum of P315; insert: (+)ESI-QqLIT-MS spectrum of P315, $[M + H]^+$ at *m/z* 316, $[M + Na]^+$ at *m/z* 338, and c) (+)ESI-QqLIT-MS^2 spectrum of P359; insert: (+)ESI-QqLIT-MS spectrum of P359, $[M + H]^+$ at *m/z* 360.

282) formed by the further oxidation of the hydroxyl group to keto group was also detected.

Further attack of RHS on the primary electrochemical oxidation products described led to the generation of their halogenated derivatives. Thus, attachment of one chloride atom at the benzene rings of P237, P281-II and P283-II yielded products P271, P315-II and P317-II. The structures of these monochlorinated oxidation by-products was elucidated by the

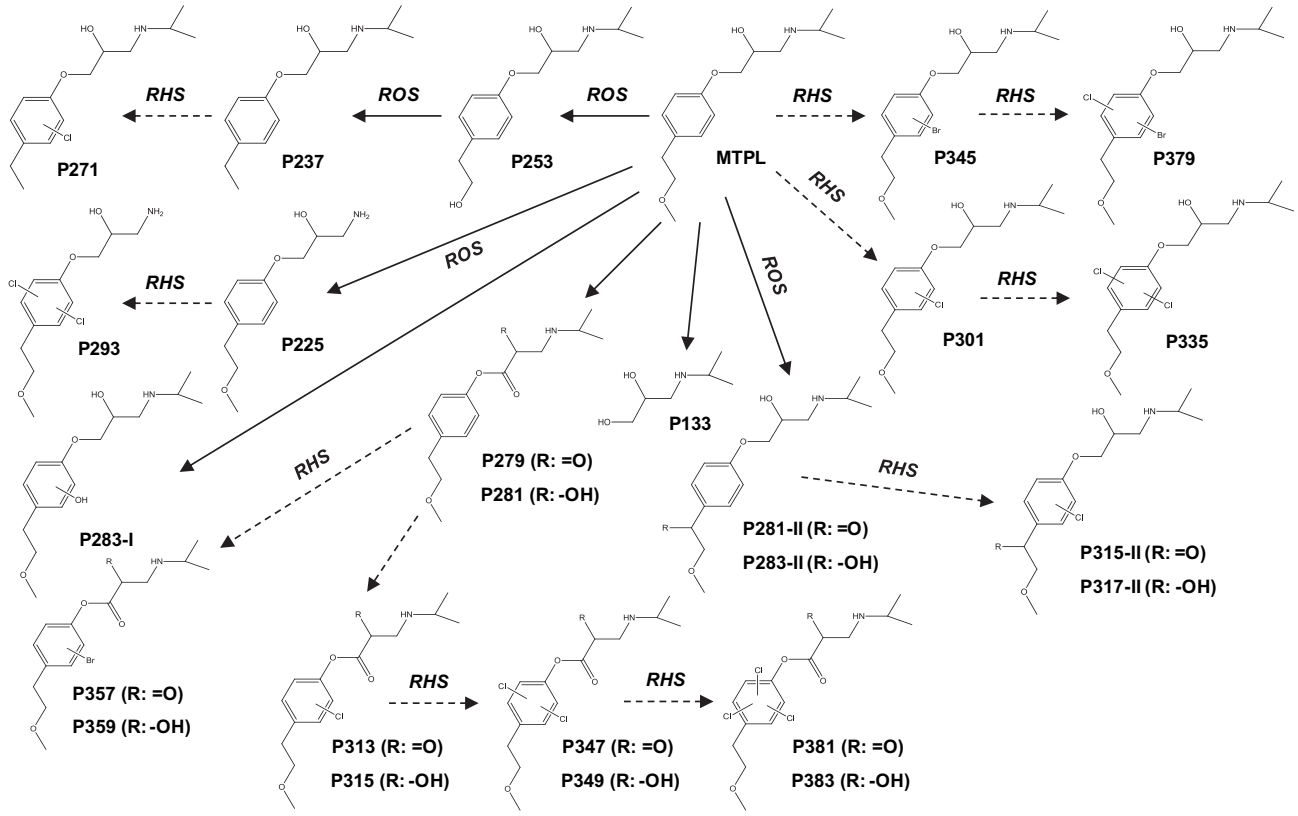

Fig. 2 – Proposed electrochemical oxidation pathways of metoprolol (MTPL) in ROC. ROS-reactive oxygen species, RHS-reactive halogen species.

fragment ions obtained in MS^2 and MS^3 scans that were shifted up for 34 Da relative to the ones observed for MTPL, and by isotope ratios and distribution in the spectra of molecular ions *m*/z 272, 316 and 318. Although the monochlorinated derivative of P225 was not found in the experiments, a strong signal appeared at $t_R = 10.6$ min with a molecular ion *m*/z 294, corresponding to the dichlorinated product P293.

Concomitantly with the disappearance of MTPL four new peaks eluted at longer t_R, exhibiting isotopic patterns characteristic for (poly)halogenated compounds. Their mass spectral comparison with MTPL revealed identical fragmentation patterns of monochlorinated (*m*/z 302, P301) and monobrominated MTPL (*m*/z 346, P345), shifted up for 34 and 78 Da, respectively. Also, CID fragmentation of the molecular ions *m*/z 336 and 380 corroborated the halogenation at the aromatic ring for products P335 and P379, identified as dichlorinated and bromo-chloro MTPL.

Another product marked as P281 (*m*/z 282) eluted at $t_R = 15.2$ min. The mass spectrum of P281 did not indicate the presence of halogens. Also, it did not coincide with the MS^2 and MS^3 fragmentation pattern of P281-II. Furthermore, appearance of product P279 (*m*/z 280, $t_R = 16.4$ min) with both –OH groups oxidized to –C=O groups implied that they were located in the side chain(s) and not at the benzene ring. Loss of water (*m*/z 264), methanol (*m*/z 250) and the isopropyl moiety (*m*/z 208) in the (+)ESI product ion mass spectra of P281 indicated that the methoxyethyl side chain remained unchanged, as well as the terminal dimethylamino group (Fig. 1a). The recorded MS^3 spectrum of the sequence *m*/z 282→208 showed an intense fragment ion *m*/z 163 formed by the loss of 45 Da (NH_3+CO), and fragment ion *m*/z 145 formed by further cleavages and intramolecular cyclization (insert in Fig. 1a). Absence of fragment ion *m*/z 116, and a strong signal observed at *m*/z 130 corroborated the assumption that the –C=O group was inserted in the α-position of ethoxy group in ethanolamide side chain. Furthermore, fragment ion *m*/z 130 was mutual for all halogenated derivatives of P281. Products P279 and P281 were further oxidized to their monochlorinated (P313 and P315), dichlorinated (P347 and P349) and brominated derivatives (P357 and P359). Additionally, low intensity peaks with molecular ions *m*/z 382 and 384 that appeared at longer oxidation time at the end of the experiment were tentatively assigned to trichlorinated by-products P381 and P383.

3.2. *Electrochemical oxidation pathway of MTPL in ROC*

The identified products allowed us to propose several electrochemical oxidation pathways of MTPL in ROC, as depicted in Fig. 2. Cleavage of terminal methyl and methoxy group in MTPL methoxyethyl side chain and formation of products P253 and P237, respectively, was achieved by the H-abstraction from the terminal, α-C atom. Besides ROS such as $OH^{\bullet}$ and O_2, $Cl_2^{\bullet-}$ and other radical RHS can also perform H-abstraction, although they are generally less reactive than $OH^{\bullet}$ (Deborde and von

Gunten, 2008). Another radical cleavage of the aromatic ether bond generated the most polar among the detected by-products, amino-diol P133, previously reported to be a radiolytic product of MTPL (Song et al., 2008). Although they are usually assigned to OH• attack, the hydroxylated products P283-I (–OH at the aromatic ring) and P283-II (–OH at the β-carbon in the methoxyethyl side chain) could have been formed by a number of ROS in the solution (e.g. $HO_2^•$, H_2O_2 and/or O_3). Further attack of ROS on the hydroxyl group resulted in the formation of P281-II. Most of the abovementioned products were previously identified as products of MTPL oxidation by OH• formed in radiolytic oxidation (Slegers et al., 2006; Song et al., 2008) and ozonation (Benner and Ternes, 2009). Scission of the aromatic ether bond and oxidative attacks at the methoxyethyl side chain by OH• were observed during electro-Fenton and photo-electron-Fenton treatment of MTPL (Isarain-Chavez et al., 2011). The most likely mechanisms of N-dealkylation (responsible for the formation of P225) in oxidation processes is by oxidative attacks at the α-C atom of the dimethylamino moiety, either by radical RHS or ROS through H-abstraction and consecutive cleavage of C–N bond, or by addition of O_2 and release of aldehyde and dealkylated amine through a carbinolamine intermediate. Considering that the secondary amine group of MTPL (pKa = 9.7) was protonated in the experimental pH range (pH 2.6–7.7), its reactivity toward both RHS and ROS can be expected to be low. Surprisingly, product P225 was very abundant and formed in slightly higher amounts on the Ti/$RuIrO_2$ anode, which is expected to produce less OH• and other radical species than Ti/SnO_2-Sb. Previously, N-dealkylated product was reported by Nouri-Nigjeh et al. (2010) as a major product of direct electrochemical oxidation of lidocaine. They explained the electrochemical N-dealkylation by the direct electron transfer from nitrogen to the anode, formation of secondary amine radical cation to give iminium intermediate, which after hydrolysis and intramolecular rearrangement leads to the formation of dealkylated amine.

The identified products P279 and P281 formed by the introduction of a carbonyl group on the α-C atom of ethoxy group were similar to α-keto-ester that was previously identified as a photocatalytic oxidation product of another β-blocker, atenolol, by accurate mass measurements using time of flight mass spectrometer (Q-ToF) (Radjenovic et al., 2009). Similar product was also observed during electrochemical oxidation of atenolol at boron-doped diamond anodes (Sires et al., 2010). These abundant products P279 and P281 were further transformed to their halogenated derivatives with –Cl and –Br substituents attached at the aromatic ring. Although the exact position of –Br and –Cl could not be determined, it is likely that it occurred in *ortho* position to the ether group which is *ortho* and *para* directing substituent. Therefore, halogenation of P279 and P281 yielded monochlorinated (P313 and P315), dichlorinated (P347 and P349), trichlorinated (P381 and P383) and monobrominated products (P357 and P359). The parent compound underwent similar transformation reactions, and MTPl-Cl (P301), MTPL-Cl_2 (P335), MTPL-Br (P345) and MTPL-BrCl (P379) were rapidly formed at the beginning of the experiment. Electrochemical oxidation products P237, P281-II and P283-II were transformed into their monochlorinated derivatives P271, P315-II and P317-II, respectively, while for dealkylated secondary amine P225 only the dichlorinated product P293 was observed.

Generally, the formation of chlorinated by-products in electrochemical oxidation is assigned to active chlorine (i.e. HClO/ClO^-) dissolved in the bulk liquid, although radical RHS formed in reactions of Cl^- and Br^- ions with OH• (e.g. $Br^•$, $Br_2^{•-}$, $Cl^•$, $Cl_2^{•-}$, and $ClBr^{•-}$) are likely play an important role (Deborde and von Gunten, 2008; De Laat and Le, 2006). Radical and non-radical RHS can be expected to be the dominant oxidizing agent under acidic conditions, decreasing the importance of OH• and other oxidants (Grebel et al., 2010). Previously, an N-chlorinated derivative was reported as the main product of MTPL chlorination in wastewater at circumneutral pH (Bedner and MacCrehan, 2006), and in aqueous solution in the pH range 5–8 (Pinkston and Sedlak, 2004). Preferential chlorination of the benzene ring is likely a consequence of protonated amine group, which is less reactive toward active chloro-species. Nevertheless, differences between the electrochemical treatment in the presence of Cl^- and aqueous chlorination could also be caused by surface electrochemical reactions, in particular adsorbed chloro and oxychloro radicals (Martinez-Huitle et al., 2005). When comparing chemical and electrochemical oxidation of phenol, Comninelis and Nerini (Comninellis and Nerini, 1995) reported that chlorinated by-products formed in the presence of hypochlorite (ClO^-) are rapidly degraded at the anode surface in the case of electrochemical oxidation. On the other hand, in spite of occurring in much lower concentrations than Cl^-, Br^- is an important scavenger of OH• (Grebel et al., 2010), and HOBr is usually more reactive than active chlorine, especially with phenolic compounds (Gallard et al., 2003). Indeed, Br-based oxidants led to the formation of brominated by-products (i.e. P345, P379, P357 and P359) in electrochemical oxidation of MTPL, despite a thousand-fold lower concentration of Br^- (1.48 mg L^{-1}) vs. 1.65 g L^{-1} of Cl^- ions in ROC. These Br-derivatives were probably formed by HOBr (and/or bromamines) formed either at the anode surface or by indirect oxidation in the bulk (e.g. by HOCl/OCl^-), although the role of Br-based radical reactions cannot be excluded (Deborde and von Gunten, 2008; Gallard et al., 2003). This is especially concerning considering that brominated by-products are suspected to be more toxic, carcinogenic and mutagenic to humans than their chlorinated analogs (Krasner et al., 2006).

3.3. *Effect of electrode coating and applied current density on the formation and distribution of by-products*

Two reaction zones of an anode can be distinguished: 1) electrochemical reaction zone (i.e. anodic surface and diffusion layer) where direct oxidation by electron transfer and/or OH• occurs, and 2) chemical reaction zone (i.e. bulk liquid) where compounds are oxidized by electrogenerated oxidant species (i.e. indirect oxidation). It is very hard to distinguish between the contribution of direct and indirect oxidation as they will be influenced by multiple factors (e.g. anode coating, current density, flow dynamic regime, waste stream matrix, reactor design). It is generally assumed that the contribution of direct electron transfer between organic matter and anode is insignificant under the conditions of high current density (Ramalho et al., 2010; Comninellis, 1994). Moreover, MTPL and its oxidation by-products will need to compete with other organic matter and inorganic ions (e.g. halides) present in ROC for adsorption and oxidation at the anode surface.

As postulated by Comninellis (Comninellis, 1994), the type of anode coating is expected to influence the electrochemical reaction pathways and by-products distribution due to different formation rates of non-selective OH• formed by water discharge. When comparing the degradation of phenol on Ti/SnO_2-Sb and Ti/RuO_2 anodes, Li et al (Li et al., 2005) explained poor performance of the latter by the shortened lifetime of $OH^•$ that hindered a more complete oxidation. On the other hand, Panizza and Cerisola (2009) demonstrated that in practice $OH^•$ accumulate only in the vicinity of a SnO_2-coated anode. Although a more significant contribution of OH• was expected for the Ti/SnO_2-Sb anode, near identical electrochemical oxidation pathways were observed for both anodes: monochlorinated P271 and dichlorinated P293 were observed only for the Ti/$RuIrO_2$ anode (Figure S21a). The appearance of these additional chlorinated by-products on Ti/$RuIrO_2$ appears rather a consequence of its lower oxidizing power (i.e. less oxidant species other than chlorine present in the bulk), than the enhanced evolution of Cl_2 at this anode. Since at the Ti/$RuIrO_2$ anode the oxygen evolution reaction (OER) takes place at lower potential this reaction is highly competitive with Cl_2 evolution, while in the case of Ti/SnO_2-Sb, the overpotential for OER is so high that the oxidation of Cl^- is kinetically favored (Ferro et al., 2000). A detrimental effect of Cl^- and Br^- ions can be expected for both $RuIrO_2$ and SnO_2-Sb coatings.

Fig. 3 illustrates qualitative profiles of MTPL and its halogenated derivatives, determined by the peak area in full-scan (+)ESI experiments and normalized to the initial peak area of MTPL (t = 0 min), plotted versus specific electrical charge consumed (Q, Ah L^{-1}) (Anglada et al., 2009). When comparing Ti/$RuIrO_2$ and Ti/SnO_2-Sb anodes under the same conditions of flow rate, pH and temperature, the generation of both halogenated and non-halogenated by-products of MTPL was enhanced on the active, $RuIrO_2$-coated electrodes. The rate of formation and disappearance of by-products was observed to be significantly faster for Ti/SnO_2-Sb anode. Similar effect was observed with the increase in current density (J) for each anode, as illustrated for Ti/$RuIrO_2$ in Figure S22, Supporting Information. In all cases, products with an inserted carbonyl group in the side chain were more abundant than their corresponding hydroxylated forms (Figures S20 b and S21). When using Ti/PbO_2 anodes, Panizza et al (Panizza et al., 2008) observed faster formation of oxidation intermediates and in

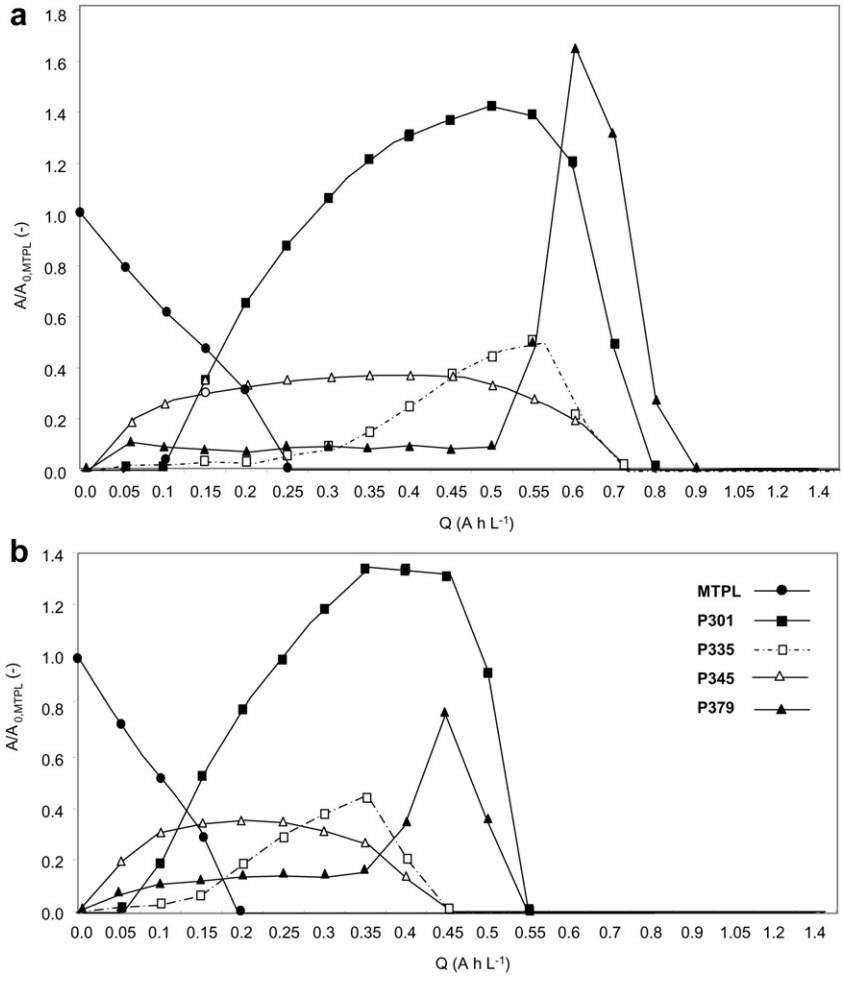

Fig. 3 – The peak areas of MTPL and its halogenated derivatives P301, P335, P345 and P379, formed during electrochemical oxidation, normalized to the initial value of the peak area of MTPL (t = 0) presented vs. Q (An h L^{-1}): a) Ti/$Ru_{0.3}Ir_{0.7}O_2$, J = 250 A m^{-2}, and b) Ti/SnO_2-Sb_2O_5, J = 250 A m^{-2}.

higher amounts, as well as their faster degradation with the increase in current density. In our study, at higher current density the accumulation of intermediates was lowered for both electrodes.

The initial pathways of electrochemical oxidation elucidated for MTPL in complex matrix of ROC seem to be identical for both electrodes and current densities applied. Enhanced competition of electrogenerated oxidants with the OER on the Ti/$RuIrO_2$ anode led to their lower concentration in the system and lower oxidation rates, which was especially evident in the case of more persistent halogenated derivatives that were very slowly degraded. On the other hand, higher amounts of oxidants promoted the oxidation steps on the Ti/SnO_2-Sb anode, and formation and generation of all by-products was shifted to lower electrical charge compared to Ti/$RuIrO_2$. However, it is unclear whether OH• plays a significant role in a complex matrix such as ROC, with high Cl^- concentrations. Several small molecular weight intermediates could be expected in OH• mediated degradation of MTPL in a chloride-free electrolyte (Isarain-Chavez et al., 2011; Sires et al., 2010). However, these products were not observed in the conducted experiments. Although Ti/SnO_2-Sb electrodes exhibit higher oxidizing power, electrogenerated OH• will rapidly be consumed by the complex matrix of ROC, primarily NOM and RHS, leaving only a small proportion of radicals for reaction with MTPL. Thus, the generation of considerable amounts of free OH• would be needed to outweigh the contribution of free chlorine and bromine, as well as various radical RHS generated (e.g. $Br_2^{\bullet-}$, $Cl_2^{\bullet-}$, $Cl^\bullet$, HClOH•/$ClOH^{\bullet-}$). Moreover, OH• will rapidly form a variety of other oxidants at the anode surface (e.g. O_2, O_3, H_2O_2), which are able to diffuse away into the bulk solution and react chemically with the organics.

3.4. *Increase in toxicity determined in* Vibrio fischeri *and* Pseudokirchneriella subcapitata *bioassays*

As the Ti/SnO_2 anode provided the fastest degradation, an additional experiment was performed with this anode to test the toxicity of the ROC after treatment. The toxicity increased substantially in both ROC alone and ROC spiked with 50 μM MTPL for all tested toxicity endpoints, apart from the direct inhibition of photosynthesis after 2 h (Text S2). The toxicity increase could be assigned to non-specific toxicity and was expressed as baseline-toxicity equivalent concentration. MTPL at 50 μM did not contribute to the mixture toxicity at all. Thus all increase in toxicity could be attributed to the transformation products, be it from MTPL degradation or from NOM degradation.

Toxicity increased linearly with the applied charge for both the spiked and unspiked samples. Baseline-TEQ are concentration additive in mixtures, therefore it was possible to subtract the contribution of the products formed during the electrochemical oxidation from the high background of increasing toxicity in the unspiked ROC sample.

Although the toxicity experiments were performed under slightly different experimental conditions than the experiments targeted for product identification, as illustrated in Figure S23, 17 out of the 25 identified products were retained and detected in the SPE sample extracts used for the bioassay analyses and all product concentrations increased during the course of the experiment. Introduction of –Cl and –Br substituents in the organic molecule are expected to augment significantly its biological activity and toxicological properties. While the transformation products were not quantified due to lack of standards, the sum of the peak areas weighted by their relative hydrophobicity relative to MTPL ($t_R/t_{R,MTPL}$) can be used as a proxy for the prediction of mixture toxicity of the identified transformation products as is explained in more detail in the Supporting Information, Text S2. This measure ($sum(A/A_{0,MTPL}{}^{*}t_R/t_{R,MTPL})$) correlates linearly with applied charge (Fig. 4), and thus the formed by-products correlate linearly with the increase in mixture toxicity. Given the good agreement of the experimental and calculated increase in toxicity, we can safely conclude that the formed products are very problematic as they cause the toxicity to increase by a factor of 40–60 times depending on the toxicity endpoint.

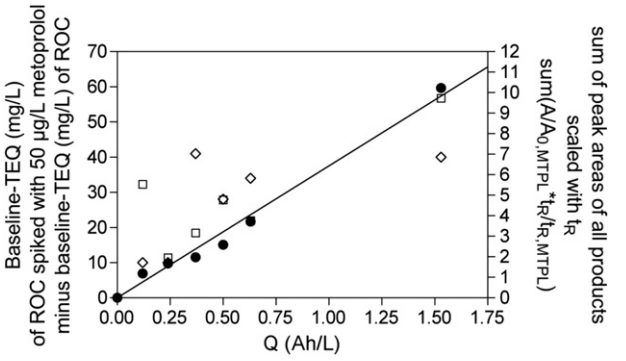

Fig. 4 – Increase in toxicity, expressed as baseline-TEQ of spiked ROC minus ROC, and sum of peak areas of the identified products (see Figure S20), scaled with the retention times in the HPLC to account for toxicity differences due to hydrophobicity as a function of the applied charge during the electrochemical oxidation experiment. □ Microtox bioassay, ◇ algae bioassay, •Sum ($A/A_{0,MTPL}{}^{*}\ t_R/t_{R,MTPL}$).

4. Conclusions

The elucidated electrochemical oxidation pathways indicate a very similar initial mechanism of degradation on the Ti/$RuIrO_2$ and Ti/SnO_2-Sb anode, with a combined effect of ROS (e.g. OH•, $O_2^{\bullet-}$, H_2O_2 and/or O_3) and RHS (e.g. HOCl, HOBr, $Br_2^{\bullet-}$, $Cl_2^{\bullet-}$, $Cl^\bullet$) on the formation and degradation of the identified oxidation by-products, likely in the bulk solution. The main differences were observed in the oxidation rates, which were always higher for the Ti/SnO_2-Sb anode. However, it is unclear whether OH• are responsible for the higher oxidizing power of the SnO_2-coated electrode when treating a complex ROC matrix with high concentrations of chloride. Further investigation is necessary to clarify the role of different oxidants produced at the anode surface and in the bulk, and establish their fate during oxidative treatment.

Nevertheless, a detrimental effect of Cl^- and Br^- was observed for both electrode coatings, with chlorinated and brominated compounds being formed either by direct attacks

of RHS on the MTPL molecule, or by further halogenation of oxidation by-products formed by ROS mediation. Furthermore, consecutive attacks of RHS at the aromatic ring yielded polychlorinated and chloro-bromo derivatives, which were even more persistent toward further oxidation and might require impractical reactor residence times to be further degraded.

Acknowledgments

This research was supported by the Australian Research Council (grant LP0989159), Veolia Water Australia, Water Secure, Magneto Special Anodes and the Urban Water Security Research Alliance. The authors would like to thank Hanne Thoen and Miroslava Macova of Entox for performing the bioassays.

Appendix. Supplementary material

Supplementary data associated with this article can be found in the online version, at doi:10.1016/j.watres.2011.03.040.

REFERENCES

Anglada, Ã, Urtiaga, A., Ortiz, I., 2009. Contributions of electrochemical oxidation to waste-water treatment: fundamentals and review of applications. J. Chem. Technol. Biotechnol. 84 (12), 1747–1755.

Anglada, Ã, Urtiaga, A., Ortiz, I., Mantzavinos, D., Diamadopoulos, E., 2011. Boron-doped diamond anodic treatment of landfill leachate: evaluation of operating variables and formation of oxidation by-products. Water Res. 45 (2), 828–838.

Bagastyo, A.Y., Radjenovic, J., Mu, Y., Rozendal, R.A., Batstone, D.J., Rabaey, K., 2011. Impact of anode material on the electrochemical oxidation of reverse osmosis membrane concentrates, Water Res., submitted.

Bedner, M., MacCrehan, W.A., 2006. Reactions of the amine-containing drugs fluoxetine and metoprolol during chlorination and dechlorination processes used in wastewater treatment. Chemosphere 65 (11), 2130–2137.

Benner, J., Ternes, T.A., 2009. Ozonation of metoprolol: elucidation of oxidation pathways and major oxidation products. Environ. Sci. Technol. 43 (14), 5472–5480.

Comninellis, C., 1994. Electrocatalysis in the electrochemical conversion/combustion of organic pollutants for waste water treatment. Electrochim. Acta 39 (11–12), 1857–1862.

Comninellis, C., Nerini, A., 1995. Anodic oxidation of phenol in the presence of NaCl for wastewater treatment. J. Appl. Electrochem. 25 (1), 23–28.

Comninellis, C., Chen, G., Kapałka, A., Fóti, G., 2010. Electrochemistry for the Environment. Springer, New York, pp. 1–23.

Deborde, M., von Gunten, U., 2008. Reactions of chlorine with inorganic and organic compounds during water treatment-kinetics and mechanisms: a critical review. Water Res. 42 (1–2), 13–51.

De Laat, J., Le, T.G., 2006. Effects of chloride ions on the iron(III)-catalyzed decomposition of hydrogen peroxide and on the efficiency of the Fenton-like oxidation process. Appl. Catal. B. Environ. 66 (1–2), 137–146.

Dialynas, E., Mantzavinos, D., Diamadopoulos, E., 2008. Advanced treatment of the reverse osmosis concentrate produced during reclamation of municipal wastewater. Water Res. 42 (18), 4603–4608.

Escher, B.I., Bramaz, N., Richter, M., Lienert, J., 2006. Comparative ecotoxicological hazard assessment of beta-blockers and their human metabolites using a mode-of-action-based test battery and a QSAR approach. Environ. Sci. Technol. 40 (23), 7402–7408.

Escher, B.I., Bramaz, N., Mueller, J.F., Quayle, P., Rutishauser, S., Vermeirssen, E.L.M., 2008. Toxic equivalent concentrations (TEQs) for baseline toxicity and specific modes of action as a tool to improve interpretation of ecotoxicity testing of environmental samples. J. Environ. Monit. 10 (5), 612–621.

Ferro, S., De Battisti, A., Duo, I., Comninellis, C., Haenni, W., Perret, A., 2000. Chlorine evolution at highly boron-doped diamond electrodes. J. Electrochem. Soc. 147 (7), 2614–2619.

Gallard, H., Pellizzari, F., Croue, J.P., Legube, B., 2003. Rate constants of reactions of bromine with phenols in aqueous solution. Water Res. 37 (12), 2883–2892.

Grebel, J.E., Pignatello, J.J., Mitch, W.A., 2010. Effect of halide ions and carbonates on organic contaminant degradation by hydroxyl radical-based advanced oxidation processes in saline waters. Environ. Sci. Technol. 44 (17), 6822–6828.

Hernando, M.D., Gomez, M.J., Aguera, A., Fernandez-Alba, A.R., 2007. LC-MS analysis of basic pharmaceuticals (beta-blockers and anti-ulcer agents) in wastewater and surface water. Trends Anal. Chem. 26 (6), 581–594.

Isarain-Chavez, E., Garrido, J.A., Rodriguez, R.M., Centellas, F., Arias, C., Cabot, P.L., Brillas, E., 2011. Mineralization of metoprolol by electro-Fenton and photoelectro-Fenton processes. J. Phys. Chem. 115 (7), 1234–1242.

Krasner, S.W., Weinberg, H.S., Richardson, S.D., Pastor, S.J., Chinn, R., Sclimenti, M.J., Onstad, G.D., Thruston Jr., A.D., 2006. Occurrence of a new generation of disinfection byproducts. Environ. Sci. Technol. 40 (23), 7175–7185.

Li, X.Y., Cui, Y.H., Feng, Y.J., Xie, Z.M., Gu, J.D., 2005. Reaction pathways and mechanisms of the electrochemical degradation of phenol on different electrodes. Water Res. 39 (10), 1972–1981.

Martinez-Huitle, C.A., Ferro, S., De Battisti, A., 2005. Electrochemical incineration in the presence of halides. Electrochem. Solid State Lett. 8 (11).

Neuwoehner, J., Escher, B.I., 2011. The pH-dependent toxicity of basic pharmaceuticals in the green algae *Scenedesmus vacuolatus* can be explained with a toxicokinetic ion-trapping model. Aquat.Toxicol. 101 (1), 266–275.

Nouri-Nigjeh, E., Permentier, H.P., Bischoff, R., Bruins, A.P., 2010. Lidocaine oxidation by electrogenerated reactive oxygen species in the light of oxidative drug metabolism. Anal. Chem. 82 (18), 7625–7633.

Panizza, M., Cerisola, G., 2009. Direct and mediated anodic oxidation of organic pollutants. Chem. Rev. 109 (12), 6541–6569.

Panizza, M., Sires, I., Cerisola, G., 2008. Anodic oxidation of mecoprop herbicide at lead dioxide. J. Appl. Electrochem 38 (7), 923–929.

Perez, G., Fernandez-Alba, A.R., Urtiaga, A.M., Ortiz, I., 2010. Electro-oxidation of reverse osmosis concentrates generated in tertiary water treatment. Water Res. 44 (9), 2763–2772.

Pinkston, K.E., Sedlak, D.L., 2004. Transformation of aromatic ether- and amine-containing pharmaceuticals during chlorine disinfection. Environ. Sci. Technol. 38 (14), 4019–4025.

Radjenovic, J., Sirtori, C., Petrovic, M., Barcelo, D., Malato, S., 2009. Solar photocatalytic degradation of persistent pharmaceuticals at pilot-scale: kinetics and characterization of major intermediate products. App. Catal. B. Environ. 89 (1–2), 255–264.

Radjenovic, J., Bagastyo, A., Rozendal, R.A., Mu, Y., Keller, J., Rabaey, K., 2010. Electrochemical oxidation of trace organic

contaminants in reverse osmosis concentrate using RuO2/IrO2-coated titanium anodes. Water Res. 45 (4), 1579–1586.
Ramalho, A.M.Z., Martínez-Huitle, C.A., Silva, D.R.d, 2010. Application of electrochemical technology for removing petroleum hydrocarbons from produced water using a DSA-type anode at different flow rates. Fuel 89 (2), 531–534.
Sires, I., Oturan, N., Oturan, M.A., 2010. Electrochemical degradation of β-blockers. Studies on single and multicomponent synthetic aqueous solutions. Water Res. 44 (10), 3109–3120.
Slegers, C., Maquille, A., Deridder, V., Sonveaux, E., Habib Jiwan, J.L., Tilquin, B., 2006. LC-MS analysis in the e-beam and gamma radiolysis of metoprolol tartrate in aqueous solution: structure elucidation and formation mechanism of radiolytic products. Radiat. Phys. Chem. 75 (9), 977–989.
Song, W., Cooper, W.J., Mezyk, S.P., Greaves, J., Peake, B.M., 2008. Free radical destruction of Î²-blockers in aqueous solution. Environ. Sci. Technol. 42 (4), 1256–1261.
Van Hege, K., Verhaege, M., Verstraete, W., 2004. Electro-oxidative abatement of low-salinity reverse osmosis membrane concentrates. Water Res. 38 (6), 1550–1558.
Wulfeck-Kleier, K.A., Ybarra, M.D., Speth, T.F., Magnuson, M.L., 2010. Factors affecting atrazine concentration and quantitative determination in chlorinated water. J. Chromatogr. A 1217 (5), 676–682.